May 2008

A membrane-based microfluidic device for controlling the flux of platelet agonists into flowing blood

Keith B. Neeves
University of Pennsylvania

Scott L. Diamond
University of Pennsylvania, sld@seas.upenn.edu

A membrane-based microfluidic device for controlling the flux of platelet agonists into flowing blood

Abstract

The flux of platelet agonists into flowing blood is a critical event in thrombosis and hemostasis. However, few *in vitro* methods exist for examining and controlling the role of platelet agonists on clot formation and stability under hemodynamic conditions. In this paper, we describe a membrane-based method for introducing a solute into flowing blood at a defined flux. The device consisted of a track-etched polycarbonate membrane reversibly sealed between two microfluidic channels; one channel contained blood flowing at a physiologically relevant shear rate, and the other channel contained the agonist(s). An analytical model described the solute flux as a function of the membrane permeability and transmembrane pressure. The model was validated using luciferase as a model solute for transmembrane pressures of 50–400 Pa. As a proof-of-concept, the weak platelet agonist ADP was introduced into whole blood flowing at 250 s^{-1} at three fluxes (1.5, 2.4, and 4.4 $\times$ 10^{-18} mol μm^{-2} s^{-1}). Platelet aggregation was monitored by fluorescence microscopy during the experiment and the morphology of aggregates was determined by post hoc confocal and electron microscopy. At the lowest flux (1.5 $\times$ 10^{-18} mol μm^{-2} s^{-1}), we observed little to no aggregation. At the higher fluxes, we observed monolayer (2.4 $\times$ 10^{-18} mol μm^{-2} s^{-1}) and multilayer (4.4 $\times$ 10-18 mol μm^{-2} s^{-1}) aggregates of platelets and found that the platelet density within an aggregate increased with increasing ADP flux. We expect this device to be a useful tool in unraveling the role of platelet agonists on clot formation and stability.

A membrane-based microfluidic device for controlling the flux of platelet agonists into flowing blood

Keith B. Neeves and Scott L. Diamond*

The flux of platelet agonists into flowing blood is a critical event in thrombosis and hemostasis. However, few *in vitro* methods exist for examining and controlling the role of platelet agonists on clot formation and stability under hemodynamic conditions. In this report, we describe a membrane-based method for introducing a solute into flowing blood at a defined flux. The device consisted of a track-etched polycarbonate membrane reversibly sealed between two microfluidic channels; one channel contained blood flowing at a physiologically relevant shear rate, and the other channel contained the agonist(s). An analytical model described the solute flux as a function of the membrane permeability and transmembrane pressure. The model was validated using luciferase as a model solute for transmembrane pressures of 50-400 Pa. As a proof-of-concept, the weak platelet agonist ADP was introduced into whole blood flowing at 250 sec^{-1} at three fluxes (1.5, 2.4, and 4.4×10^{-18} mol µm^{-2} sec^{-1}). Platelet aggregation was monitored by fluorescence microscopy during the experiment and the morphology of aggregates was determined by *post hoc* confocal and electron microscopy. At the lowest flux (1.5×10^{-18} mol µm^{-2} sec^{-1}), we observed little to no aggregation. At the higher fluxes, we observed monolayer (2.4×10^{-18} mol µm^{-2} sec^{-1}) and multilayer (4.4×10^{-18} mol µm^{-2} sec^{-1}) aggregates of platelets and found that the platelet density within an aggregate increased with increasing ADP flux. We expect this device to be a useful tool in unraveling the role of platelet agonists on clot formation and stability.

1. Introduction

During thrombus formation on the exposed subendothelial matrix, platelets pause or roll on von Willebrand factor, and then arrest and activate on collagen[1, 2]. Adhered platelets become activated through outside-in signaling via glycoprotein receptors[3]. Activated platelets recruit and aggregate other platelets by producing soluble agonists and releasing them into the flowing blood. These agonists include, but are not limited to, thrombin[4], ADP[5], and thromboxane A_2[6]. The cellular and molecular events of platelet adhesion to surface-bound proteins and subsequent platelet activation has been extensively studied in animal[7-9] and *in vitro* models[10-14]. *In vitro* models have been critical in defining the shear dependent bonding dynamics between platelet receptors and their surface bound ligands. Parameters such as on and off rates and adhesion efficiency have been measured by manipulating the composition and density of surface-bound ligands[15]. However, there are no *in vitro* models for manipulating agonist flux into flowing blood.

In this report, we describe a membrane based microfluidic device for controlling the flux of platelet agonists into flowing whole blood. The device consists of two channels separated by a membrane. One channel contains blood flowing at a physiologically relevant mean wall shear rate (250-2000 sec^{-1}). The second channel, containing the agonist(s), is oriented perpendicular to the first channel. At the intersection of the two channels, the flux of agonists into flowing blood is controlled by the concentration of the agonist and the transmembrane pressure. Luciferase was used as a model solute to examine the roles of wall shear rate, the relative flow rates of the two channels, and protein fouling on flux. Analytical and numerical models were developed to describe the fluid flow and mass transport in the device. As a proof-of-concept, the platelet agonist ADP was introduced at three different molar fluxes into flowing whole blood. *Post hoc* electron and confocal microscopy reveal that platelet activation and aggregation depend on the magnitude of ADP flux. This is the first demonstration of user-controlled ADP wall flux into flowing blood to trigger platelet deposition.

2. Experimental

2.1 Device fabrication and operation

Figure 1a illustrates the three layers of the device; 1) a top channel that contains flowing blood, 2) a track-etched polycarbonate membrane, and 3) a bottom channel that contains the agonist solution and a vacuum chamber. The channels were made by (poly)dimethlysiloxane (PDMS) molding techniques[16]. Briefly, a high aspect ratio negative photoresist (KMPR 1050, MicroChem Corp., Newton, MA) was spun and patterned on a silicon substrate at a height of 100 µm. Microfluidic channels had a cross-sectional area of 100 µm × 100 µm. In the bottom layer the channel was separated by a solid barrier from the vacuum chamber. An array of 400 µm posts spaced 1 mm apart was used to prevent collapse of the vacuum chamber under negative pressure (Figure 1c). The bottom channel was a single mold process,

PDMS mold off of a photoresist master. The top channel and vacuum chamber required a two mold process, with an additional PDMS mold off a PDMS master. We found the two mold process to provide better pattern transfer of the pillars than a single mold process. Inlet and outlet holes were created in the PDMS using sharpened 23 gauge stainless steel tubing. Small diameter tubing (PEEK, ID=150 µm, OD=360 µm, Upchurch Scientific, Oak Harbor, WA) was used to make external connections to reservoirs of agonist(s) and blood solutions and withdrawal syringes. A compression fitting for connection to the PDMS was made by gluing a larger diameter sleeve (PEEK, ID=380 µm, OD=1/16 inch) over the end of the small diameter tubing. One foot of tubing was used for all four connections, inlet and outlet of both channels. The total dead volume in the tubing for each channel was 11 µL. The flow rate of the top and bottom channels were independently controlled with two syringe pumps (PHD 2000, Harvard Apparatus, Holliston, MA) driving glass syringes (100 µL and 250 µL, Hamilton Co. Reno, NV). The device was assembled by placing a track-etched polycarbonate membrane (13 mm diameter, B1013-MB, Structure Probe, Inc., West Chester, PA) onto a 10 mm platform on the bottom PDMS layer. The bottom and top layers were aligned by hand using a low magnification stereoscope, brought into contact, and vacuum sealed at a pressure of ~40 kPa using a diaphragm pump (DOA-V163-BN, Gast Manufacturing, Inc., Benton Harbor, MI). By design, there was a thin gap between the two PDMS layers at the periphery of the membrane. During the flow experiments, fluid slowly escaped through this gap into the vacuum chamber. Less than 10 µL of fluid was lost through the gap over one hour. Since the membrane area is larger than the PDMS platform there is no cross-contamination between the two fluid streams. At high wall shear rates (1000-2000 sec^{-1}) both the blood and agonist reservoirs were at atmospheric pressure and were withdrawn (negative pressure) via the syringe pumps. In some experiments at low all shear rates (250-500 sec^{-1}), the agonist solution was infused (positive pressure) and the blood solution withdrawn (negative pressure) to a achieve higher transmembrane pressure.

2.2 Agonist flux models

Solute flux through the membrane into a flowing solution is determined by the solute properties (size, shape, charge), the pore characteristics of the membrane (radius, length, pore density), and the operating conditions (concentration gradients and pressure gradients). Within the blood containing channel, the constant flux of agonist leads to the formation of a boundary layer which begins at the upstream edge of the reaction zone. The thickness of the boundary layer determines how many platelets experience threshold concentrations of an agonist and thus are activated. We developed two models to capture each of these events; 1) an analytical model which describe the flux of a solute through the membrane and 2) a finite element model to capture the fluid dynamics and transport within the microfluidic channels.

2.2.1 Analytical Model of Agonist Flux

As a first-order estimate, we treated the membrane as a porous medium that uniformly experiences the same pressure drop across the entire length and width of the membrane (100 µm × 100 µm) at the intersection between the two channels. The transmembrane pressure was obtained by first calculating the pressure in each channel and then subtracting the difference between the two channels at the intersection point. Owing to the small diameter of the PEEK tubing used in the experiments, we also accounted for the pressure drop through the tubing, which in some cases was a significant fraction of the overall pressure drop. We analytical expressions to find the pressure drop through a rectangular channel per unit length and the wall shear rate[17]:

$$\frac{P}{L} = \frac{\bar{v}\mu}{h^2}\left[\frac{1}{3} - \frac{64\varepsilon}{\pi^5}\tanh(\pi/2\varepsilon)\right]^{-1} \quad (1)$$

where P is pressure, L is channel length, $\bar{v}$ is the mean velocity, μ is viscosity, h is channel height, ε is the channel aspect ratio. The mean velocity was set to achieve a desired mean wall shear rate:

$$\bar{v} = \frac{2\gamma_{wall}\sqrt{A}}{f\,\mathrm{Re}} \quad (2)$$

$$f\,\mathrm{Re} = \frac{12}{\left(1 - \frac{192}{\pi^5}\varepsilon\tanh(\pi/2\varepsilon)\right)(1+\varepsilon)\sqrt{\varepsilon}} \quad (3)$$

where γ_{wall} is the mean wall shear rate, A is the channel cross-sectional area, f is the Fanning friction factor, and Re is the Reynolds number based on a characteristic length of $\sqrt{A}$. To find the transmembrane pressure, eq. 1 was evaluated at the half length of both channels (including tubing):

$$\Delta P_{membrane} = P_{1,L/2} - P_{2,L/2} \quad (4)$$

where $\Delta P_{membrane}$ is the transmembrane pressure, and $P_{1,L/2}$ and $P2_{,L/2}$ is the pressure in channel 1 and 2, respectively, at the half length of the channel. The specific discharge of agonist from channel 2 into channel 1 was calculated using Darcy's law and the experimentally determined hydraulic permeability (see section 2.3.1):

$$v_a = -\frac{k}{\mu}\frac{\Delta P_{membrane}}{t} \quad (5)$$

where v_a is the agonist velocity through a single pore, k is the Darcy's permeability, and t is the membrane thickness. The unhindered agonist flux was calculated by considering both diffusive and convective transport through the membrane:

$$J_a = -D_\infty\nabla c_a + v_a c_a \quad (6)$$

where J_a is the agonist flux, D_∞ is the agonist diffusion coefficient in water, c_a is the agonist concentration, and v_a is the mean velocity. In the membranes used in this report the agonist was much smaller than the pore ($r_{agonist}/r_{pore} < 0.01$), so there were no steric hindrances to transport[18]. We assume that

the concentration in the top channel is zero, so that the concentration gradient across the membrane is $\nabla c_a=(c_{a,2}-0)/L$. This assumption overestimates the agonist flux because the concentration at the wall in the top channel is nonzero. However, in most cases the device is operated at a pore Peclet number ($Pe=v_aL/D$) greater than 10 and therefore the contribution of the diffusive flux to the overall flux is small (<10%).

2.2.2 Finite Element Model of Agonist Flux and Distribution

A two-dimensional model of fluid flow and agonist transport was developed using commercial finite element software (COMSOL Multiphysics, Burlington, MA). The model geometry consists of two parallel channels, each with a height of 100 µm and a length of 18.5 mm, connected by a membrane at the half-length. The membrane was modeled as a porous medium with a Darcy's permeability of 3690 nm^2 (Table 1). The fluid in the top layer had the density (1060 kg m^{-3}) and viscosity (0.004 Pa s) of whole blood[19], but does not account for the volume excluded by blood cells. The solution in the bottom channel had the physical properties of water and the diffusivity of ADP was estimated using the Wilke-Chang correlation[20].

The mesh consisted of 303,616 triangular elements. Mesh independence was evaluated by comparing the concentration profiles for grids consisting of 206,436, 303,616 and 375,122 elements. There was no greater than 2% difference in the magnitude of the concentration between the three grid sizes at any position within the simulation geometry. The steady state mass and momentum conservation equations were solved in 28 minutes using a linear systems solver (UMFPACK) on a Linux workstation (dual 2.2 GHz processors, 12 GB RAM).

2.3 Device characterization

2.3.1 Membrane hydraulic permeability

The hydraulic permeability for membranes with a pore diameter of 0.6 µm and 1 µm and three surface conditions (no coating, BSA coated, fibrinogen coated) was determined by measuring the flow rate through the membrane under a constant pressure head. Protein coatings were achieved by incubation of 1 mg/ml BSA or 0.1 mg/ml fibrinogen for two hours at room temperature followed by thorough rinsing in deionized water. Wet membranes were mounted in a filter holder (F0101-BA, Structure Probe Inc., West Chester, PA, USA). A constant pressure head was provided in a 60 mL syringe attached to the top of the filter holder. The flow rate was determined by measuring the weight of the permeating deionized water after 5 minutes on a top loading balance.

Water levels of 1.5, 2, and 2.5 inches of water (373, 500, 627 Pa) were maintained for 5 minutes for 0.6 µm membranes. Water levels of 1.5, 2, and 3 inches of water (373, 500, 750 Pa) were maintained for 5 minutes for 0.6 µm membranes. Each measurement was performed in triplicate with a different membrane. These pressure drops are comparable to those across the membrane within the device. Using Darcy's Law ($v=k/\mu\nabla P$), the permeability was calculated by a least square fit of the data Q/A versus P/t, where Q is the flow rate in m^3/s, A is the membrane area in m^3, P is the pressure drop in Pa, and t is the thickness in m.

Previous reports showed that water flux decreases with time for track-etched polycarbonate membranes. In a second set of experiments, we measured the permeability as function of time over 25 minutes at each pressure (250, 500, 750 Pa).

2.3.2 Luciferase molar flux

The molar flux was adjusted by changing the wall shear rate in the top channel, the relative flow rate (Q1/Q2), and agonist concentration. We used firefly luciferase (61 kDa) as model agonist and measured the flux through a polycarbonate membrane with an average pore diameter of 1 µm. The flow rate in the top channel was set to mean wall shear rates of 250, 500, 1000, and 2000 sec^{-1} to represent the range of venous to arterial shear rates. The relative flow rate between the top and bottom channel (Q1/Q2) was varied over a range of 0.075-25. In experiments where Q1/Q2>1, fluid was withdrawn from both channels. In experiments where Q1/Q2<1, fluid was withdrawn from the top channel and infused into the bottom channel. The fluid in the top channel was 1 mg/mL bovine serum albumin (BSA) (Sigma, St. Louis, MO) in phosphate buffered saline (PBS). The fluid in the bottom channel was 1 nM or 10 nM luciferase and 1 mg/mL BSA in PBS. The BSA helped minimize adsorption of the luciferase to PDMS. Before each experiment the channels and membrane were incubated in a 1 mg/mL BSA solution for one hour to minimize nonspecific protein adsorption.

For each experiment, a total of 100 µL of fluid was collected from the top channel. Following the experiment, 20 µL aliquots of fluid from both channels were transferred into white 96-well plates in triplicate for each experimental condition. Luciferase concentration was determined by flash luminescence using a plate reader (2103 Envision, PerkinElmer, Waltham, MA). An automated dispenser in the plate reader injected each well with 100 µL of substrate (E4550, Promega Corp., Madison, WI) followed immediately by reading the luminescence signal for 10 seconds. Luciferase concentration was calculated by integrating the luminescence signal for nine seconds and comparing the integrated signal to a standard curve. A standard curve was generated for each plate over the linear range (10 fM to 1 nM) of the luminescence assay. The luciferase flux was calculated by multiplying the concentration by the flow rate and dividing by the cross-sectional area (100 µm × 100 µm) where the two channels intersect. Each experimental condition was run in triplicate on a separate membrane.

Membranes used for protein filtration are known to foul over time, which can lead to diminished water and solute flux[21, 22]. We investigated the role of fouling in this system by measuring luciferase flux at different transmembrane pressures over 25 minutes. The experimental conditions were 1 nM luciferase and 1 mg/mL BSA in PBS in the bottom channel, 1 mg/mL BSA in PBS in the bottom channel, Q1/Q2=10 for mean wall shear rates of 2000 sec^{-1} and 1000 sec^{-1}, Q1/Q2=0.5 for mean wall shear rates of 500 sec^{-1} and 250 sec^{-1} in the top channel. Fractions were collected every 5 minutes, diluted to a total volume of 100 µL, and the flux was determined following the procedure above.

2.4 Introduction of ADP into flowing whole blood

Human whole blood was obtained from healthy volunteers via venipuncture and anticoagulated with sodium citrate (9 parts blood to 1 part sodium citrate) and corn trypsin inhibitor (50 μg/ml final concentration) to block Factor XIIa and associated intrinsic pathway initiation. Platelets were incubated for five minutes with an anti-CD41:Alexa 647 antibody (MCU467A647, AbD Serotec, Releigh, NC) at a volume ratio of 50 parts blood to 1 part antibody. Immediately before introduction into the device, the blood was recalcified with CaCl$_2$ (100mM in HEPES buffered saline) to a final calcium concentration of 20 mM. The blood was withdrawn to achieve a mean wall shear rate of 250 sec^{-1} for five minutes. ADP (10 μM) in HEPES buffered saline (HBS) was perfused at relative flow rates of Q1/Q2=0.075, 0.15, 0.3 corresponding to transmembrane pressures of 1020, 545, and 308 Pa, respectively. After five minutes, the blood was replaced with HBS and the adhered platelets were washed for five minutes at a mean wall shear rate of 100 sec^{-1}. Each experimental condition was run in triplicate with blood from a different donor. The platelet count for each donor was measured using a Coulter counter.

The device was operated as described in section 2.3.2, except that the polycarbonate membrane was incubated in 0.1 mg/mL human fibrinogen for 2 hours. Adsorbed fibrinogen is amenable to activated platelet adhesion through the $\alpha_{IIb}\beta_3$ integrin, but does not result in quiescent platelet adhesion at the shear rates in this report[23]. Before introducing blood and agonists into the device, the channels were filled with 1 mg/ml BSA solution in HBS buffer and allowed to flow for 10 minutes at Q1/Q2=1.

2.5 *Post hoc* electron and confocal microscopy

Immediately following a flow experiment, the device was dismantled and the membrane was thoroughly washed in HBS buffer. The sample was fixed in 2% glutaraldehyde for four hours at room temperature and overnight at 4 ºC. The samples were stored in 0.1 M sodium cacodylate buffer at 4 ºC until processing. The day of imaging, the samples were dehydrated for 15 minutes in graded ethanol solutions of 50%, 70%, 80%, 90%, and twice in 100%. For electron microscopy, the samples were then critical point dried and sputtered with Au/Pd. Samples were imaged on a field emission scanning electron microscope (Supra 50VP, Carl Zeiss SMT, Oberkochen, Germany) at an accelerating voltage of 5 kV. For fluorescence microscopy, the samples were coverslipped in mounting medium (H-100, Vector Laboratories, Burlingame, CA) and imaged using a 60x oil immersion objective on a spinning disk confocal fluorescence microscope (IX81-DSU, Olympus America, Center Valley, PA).

To estimate the role of ADP flux on platelet aggregation, we calculated the platelet surface and volume density in aggregates for the different experimental conditions. For each membrane, the integrated fluorescence intensity of single platelets (n=10) was measured as a baseline value (F$_o$). The integrated fluorescence intensity of each aggregate (F$_a$) was divided by the baseline single platelet value to yield the number of platelets per aggregate (N=F$_a$/F$_o$). We defined the platelet surface density as the number of platelets per

aggregate divided by the aggregate area ($\bar{N}$ =N/A$_a$). We only considered platelet aggregates formed in the first 200 μm downstream from the reaction zone. The platelet volume density within an aggregate was measured by dividing the surface density by the confocal stack height, which ranged from 4-8 μm.

3 Results

3.1 Device Characterization

A three layer device consisting of two perpendicular channels and a membrane was fabricated for controlling the flux of platelet agonists into blood flowing at physiological shear rates (Figure 1). The three layers were reversibly sealed during operation by vacuum-assisted bonding. The agonist flux was a function of the membrane properties, the relative flow rate of the two channels (Q1/Q2), and the agonist concentration in the bottom channel.

3.1.1 Membrane hydraulic permeability

The permeability was measured for track-etched polycarbonate membranes with pore diameter of 0.6 and 1 μm. Table 1 shows the permeability of membranes with these two pore diameters for no surface treatment, adsorbed BSA, and adsorbed fibrinogen. Figure S1 shows the velocity as a function of pressure and least squares fit used to determine permeability. There is approximately a four-fold smaller permeability of the 0.6 μm pore membranes than the 1.0 μm pore membrane (k$_{1\mu m}$/k$_{0.6\mu m}$≈4). For a porous medium with straight cylindrical pores, like track-etch polycarbonate, the permeability is proportional to the pore density and the pore diameter to the fourth power (k α N d$_{pore}^4$)[24]. The manufacturer reports a pore density of 2×10^7 pores/cm^2 for 1 μm pore diameter membranes and 3×10^7 pores/cm^2 for 0.6 μm pore diameter membranes. Therefore, the ratio of the permeabilities between the two membranes should be k$_{1\mu m}$/k$_{0.6\mu m}$=5.1. However, this estimate does not account for dispersity of pore sizes and non-parallel pores, both of which could lead to a lower permeability.

For a pore diameter of 1 μm there was no significant change in the permeability for all three surface conditions. There was a 43% decrease in permeability for fibrinogen treated 0.6 μm pore membranes and no change for BSA-treated membranes. Based on these results, we chose to use the 1 μm pore membranes for device characterization and blood experiments since there was no change in permeability between BSA and fibrinogen surface treatments.

Previous reports have shown a decrease in water flux with time for track-etched polycarbonate membranes[24, 25]. Figure S2 shows the decline in water flow rate for membranes with a 1 μm average pore diameter as function fo time. For constant pressure heads of 250, 500, and 750 Pa there was a 11.0%, 10.5%, and 4.4% decline in water flux over 25 minutes, respectively. The flux decline may be due to particulates in the water and bubbles forming within the pores. Mueller and Davis reported a 41-60% water flux decline in track-etched polycarbonate membranesover the same time, albeit for smaller pores (0.2 mm) and much larger pressures (69,000-138,000 Pa)[25].

3.1.2 Luciferase molar flux

The agonist flux was manipulated by varying three parameters; relative flow rate, wall shear rate, and agonist concentration. Varying the relative flow rate and wall shear rate were both methods for changing the pressure drop across the membrane. Varying the agonist concentration changed the concentration gradient between the two channels. Figure 2a shows the luciferase flux as function of the relative flow rate ($Q1/Q2$) for a mean wall shear rate of 1000 sec^{-1} and 2000 sec^{-1} in the top channel. The luciferase flux was modulated by almost one order of magnitude at 2000 sec^{-1} by changing the relative flow rate from 1 to 25. Decreasing the flow rate in the bottom channel (agonist) to less than 10% of the flow rate in the top channel results in negligible changes in agonist flux. The analytical model qualitatively describes the trend measured in the data, but tends to underestimate the agonist flux by 10-20% at these wall shear rates.

Figure 2b shows the decline in luciferase flux as a function of time for four wall shear rates. The mean wall shear rates were 2000, 1000, 500, and 250 sec^{-1}, which corresponded to transmembrane pressures of 550, 275, 120, and 60 Pa. Over a 25 minute experiment there was an average luciferase flux decline of 50% (550 Pa), 37% (275 Pa), 40% (120 Pa), and 49% (60 Pa). Mueller and Davis reported a 98% decline in BSA flux (feed concentration 1 mg/mL) over the same time in a 0.2 mm pore polycarbonate membrane for a transmembrane pressure of 138,000 Pa[25]. Similar to our results, they did not find the transmembrane pressure to affect the rate of fouling.

Figure 2c compares the experimental flux to the theoretical flux ($k=3690$ nm^2) from the analytical model developed in Section 2.2.1. The flux depends linearly on transmembrane as predicted by eqn. 6 for all times, however the model does not describe the change in permeability as a function of time. Since the percent decline was similar for all pressures, there was significantly larger changes in the magnitude of the flux at higher transmembrane pressures. This fact was most evident at a transmembrane pressure of 550 Pa, the where model underestimates flux at early times and overestimated flux at late times.

3.2 Platelet aggregation as a function of ADP flux

ADP (10 µM) was introduced at relative flow rates of 0.075, 0.15, and 0.3 into whole blood flowing at a mean wall shear rate of 250 sec^{-1} over a fibrinogen coated membrane. These relative flow rates correspond to ADP molar fluxes of 4.4, 2.4, 1.5 × 10^{-18} mol μm^{-2} sec^{-1} (eq. 6), respectively. Identical experimental conditions using an ADP feed concentration fo 1 µM resulted in negligible platelet adhesion.

The adhesion and aggregation of platelets was monitored in real-time using fluorescence microscopy (Figure 3). Imaging through several layers of material (glass, PDMS, and polycarbonate) diminished the resolution of images, but nevertheless allowed for real-time monitoring of platelets adehsion. Individual platelets were resolved at early times (Figure 3a). A possible improvement of the device is to replace the bottom PDMS layers with channels etched in glass, thereby removing a layer and improving resolution.

Following the experiment, the membrane was removed from the device and prepared for either electron or confocal microscopy. Figure 4 demonstrates that the area and height of platelet aggregates depends on ADP flux. There were no platelet aggregates formed at the lowest ADP flux. Aggregates of 20-250 platelets were observed at an ADP flux of 2.4 × 10^{-18} mol μm^{-2} sec^{-1}. These aggregates tended to be monolayers and had a platelet surface density of 0.21±0.05 platelets μm^{-2} (n=24) and an average volume density of 5.22 × 10^7 platelets μL^{-1}. Aggregates of 75-1000 platelets were observed at an ADP flux of 4.4 × 10^{-18} mol μm^{-2} sec^{-1}. These aggregates often contained multiple layers of platelets and had a platelet surface density of 0.31±0.04 platelets μm^{-2} (n=11) and an average volume density of 3.45 × 10^7 platelets μL^{-1}. The volume density of platelets within aggregates was 174 fold and 115 fold greater than the average platelet plasma density for an ADP flux of 4.4 × 10^{-18} mol μm^{-2} sec^{-1} and 2.4 × 10^{-18} mol μm^{-2} sec^{-1}, respectively.

Observations from electron microscopy of aggregates show that the morphology of platelets was qualitatively different at a higher ADP flux (Figure 5). At the lowest ADP flux ($Q1/Q2=0.3$), platelets adhered only to the 100 µm × 100 µm reaction zone where the two channels intersected. In addition, most of these platelets maintained their quiescent discoid shape and did not form aggregates (Figure 5a). At the middle ADP flux ($Q1/Q2=0.15$), platelet adhesion was not limited to the reaction zone and aggregates were observed up to one millimeter downstream from the reaction zone. The presence of filopodia protruding from cell bodies and platelet-platelet tethers clearly indicates activated platelets (Figure 5b).

The size and height of platelet aggregates increased with increasing ADP flux as expected from consideration of the ADP distribution in the top channel. A boundary layer of ADP begins to form at the upstream edge of the membrane and grows over the length of the membrane (Figure 6a). Downstream from the membrane, the boundary layer begins to dissipate by diffusion into the bulk solution. The thickness of the boundary layer depends on the ADP flux through the membrane. Figure 6b illustrates this dependence for the three operating conditions considered in the ADP experiments. As the flux increases, the thickness of the boundary layer increases, and therefore more flowing platelets are activated and aggregate. At the middle ADP flux (2.4 × 10^{-18} mol μm^{-2} sec^{-1}) most of the aggregates were monolayers of platelets, whereas at the high ADP flux (4.4 × 10^{-18} mol μm^{-2} sec^{-1}) there were several multilayer aggregates.

4 Discussion

Platelet adhesion to surface-bound protein on the subendothelium is the *initial condition* of blood coagulation. Following adhesion, the platelets become activated and in turn generate thrombin and thromboxane A_2 on their extracellular membranes and release ADP from intracellular stores to promote further platelet activation and aggregation. The release of these platelet agonists into the blood flowing over the adhered platelets is the *boundary condition* that leads to platelet aggregation. The flux of these three agonists into flowing blood serves an important role in thrombosis and hemostasis. However, the combined function of such soluble

agonists during clot formation under flow is unknown, since no method allows controlled fluxes of agonists into flowing blood. The relationship between solute flux and stable clot formation is a complex reaction-transport problem with coupled particle deposition. One example of altered solute flux is hemophilia, where deficiencies in clotting factors attenuates thrombin generation[26], which leads to unstable clots[27]. It is less clear whether these clots are unstable because of diminished fibrin formation or diminished platelet activation, or both. The device described in this report provides a method for manipulating solute flux that could be useful for studying hemophilia and other bleeding disorders.

The size and growth of a thrombus is limited by the interplay between activated platelets and intact endothelial cells. Endothelial cells secrete soluble molecules (nitric oxide, prostacyclin, ecto-necleotidases) that control platelet reactivity in a process known as thromboregulation[28]. The device presented in this report could be extended to study thromboregulation with additional bottom channels for introduction of these platelet antagonists.

Incorporation of membranes into microfluidic devices is becoming increasingly common for on-chip filtration and separations, as well as a component for sensors, reactors, and cell culture[29]. In this report we incorporated commercially available membranes as fluidic resistor into a microfluidic device by modifying a technique first reported by Ismagilov and colleagues[30]. This technique has been employed for screening biochemical interaction[30], generating chemical gradients[31], and monitoring communication between different cell types[32]. A notable modification we have made was the use of vacuum assisted bonding[33]. This reversible bonding technique allowed for *post hoc* morphological analysis of platelet aggregates by electron and spinning disk confocal microscopy.

Track-etched polycarbonate membranes demonstrate both internal and external fouling under different operating conditions[24, 25, 34]. Internal fouling describes the adsorption and deposition of molecules and particles onto the surface of the pore, and consequently reducing the pore size. External fouling describes the accumulation of larger particles and cells that cannot enter pores. We have chosen a membrane whose pores are much larger than any of the solutes we are interested in introducing into blood, but also small enough to exclude blood cells. However, we still observed fouling of the pores that lead to significant flux decline over 25 minutes. This flux decline was most likely the result of internal fouling based on moderate transmembrane pressures and short length of the experiments[25]. Other choices of membranes include cellulose acetate, polyvinylidene fluoride, or polysulfone. However, these other membranes have a minimum thickness on the order of 100's microns, whereas the polycarbonate membranes are 5-15 μm thick. The membrane thickness is an important parameter in the multilayer device described in the manuscript. We attempted to use a cellulose acetate membrane (thickness=110 μm) and found that the loss of fluid into the vacuum chamber was prohibitive.

Solute transport was accurately predicted with an analytical model when convection was the dominant transport mechanism within the pores (Pe>10). Although the model did not account for protein fouling, it was a good first-order etstimate of flux that only required two parameters, the membrane permeability and transmembrane pressure. The device was operated in two configurations that depended on the wall shear rate in the top channel. At higher wall shear rates (1000-2000 sec⁻¹), there was a large enough transmembrane pressure generated by the top channel to achieve predominantly convective transport in the pores. At these high shear rates, fluid was withdrawn (negative pressure) from both channels. At lower wall shear rates (250-500 sec⁻¹), the transmembrane pressure generated by the top channel was insufficient to ensure convective transport. Therefore, at these low shear rates, the bottom channel was infused (positive pressure) to compensate for small pressure drop in the top channel. In some applications, such as gradient generation, diffusion-mediated transport may be preferable. This mode of operation is achievable by withdrawing fluid from both channels at the same flow rate, provided the channels have the same length and cross-sectional area.

As a demonstration of the device, we examined the dependence of platelet aggregation on ADP flux. We observed that platelet activation, aggregation size, and aggregation height depended on the magnitude of ADP flux. At the lowest ADP flux considered, there was sparse adhesion of platelets and little evidence of aggregation and platelet-platelet tethering. At the higher fluxes, we observed aggregates of hundreds of activated platelets. The size and height of aggregates increased with increasing ADP flux. These observations agree with previous reports that platelet adhesion efficiency to fibrinogen coated surfaces increases with ADP induced activation[23]. In addition, computational studies predict that a thicker agonist boundary layer yields greater platelet aggregation[35-37]. In these computational studies, boundary layer thickness and thus platelet aggregation was modulated by changing the wall shear rate. However, increasing the agonist flux has a similar effect to decreasing the wall shear rate.

5 Conclusions

We have fabricated and characterized a membrane-based microfluidic device for controlling the flux of platelet agonists into flowing blood. The molar flux of luciferase was accurately predicted at high pore Peclet numbers using an analytical model. The introduction of ADP ($1.5\text{-}4.4 \times 10^{-18}$ mol μm⁻² sec⁻¹) into flowing whole blood resulted in flux dependent platelet aggregation and activation. We expect this device will be a useful tool in unraveling the role of platelet agonists on clot formation and stability.

Notes and references

5 *1050 Vagelos Laboratories, Dept. of Chemical and Biomolecular Engineering and Institute for Medicine and Engineering, University of Pennsylvania, Philadelphia, PA 19104, USA Fax: 01 215 573 6815; Tel:01 215 573 5704 E-mail:sld@seas.upenn.edu.*

10 † Electronic Supplementary Information (ESI) available: [Figures of the measurement of hydraulic permeabilities and water flux in polycarbonate membranes.]. See DOI: 10.1039/b000000x/

1. V. T. Turitto, H. J. Weiss, T. S. Zimmerman and I. I. Sussman,
15   *Blood*, 1985, **65**, 823-831.
2. J. J. Sixma, G. H. van Zanten, E. U. Saelman, M. Verkleij, H. Lankhof, H. K. Nieuwenhuis and P. G. de Groot, *Thromb. Haemost.*, 1995, **74**, 454-459.
3. M. L. Kahn, *Semin. Thromb. Hemost.*, 2004, **30**.
20 4. S. R. Coughlin, *Nature*, 2000, **407**, 258-264.
5. C. Gachet, *Ann. Med.*, 2000, **32 Suppl 1**, 15-20.
6. B. Z. S. Paul, J. Jin and S. P. Kunapuli, *J. Biol. Chem.*, 1999, **274**, 29103-29114.
7. E. D. Rosen, S. Raymond, A. Zollman, F. Noria, M. Sandoval-
25   Cooper, A. Shulman, J. L. Merz and F. J. Castellino, *Am. J. Pathol.*, 2001, **158**, 1613-1622.
8. S. Falati, P. Gross, G. Merrill-Skoloff, B. C. Furie and B. Furie, *Nat. Med.*, 2002, **8**, 1175-1180.
9. E. R. Vandendries, J. R. Hamilton, S. R. Couglin, B. Furie and B. C.
30   Furie, *Proc. Natl. Acad. Sci. U. S. A.*, 2007, **104**, 288-292.
10. W. R. Wagner and J. A. Hubbell, *J. Lab. Clin. Med.*, 1990, **116**, 636-650.
11. J. M. Ross, L. V. McIntire, J. L. Moake and J. H. Rand, *Blood*, 1995, **85**, 1826-1835.
35 12. V. Balasubramanian, E. Grabowski, A. Bini and Y. Nemerson, *Blood*, 2002, **100**, 2787-2792.
13. M. Goel and S. L. Diamond, *J. Thromb. Haem.*, 2004, **2**, 1402-1410.
14. U. M. Okorie and S. L. Diamond, *Biophys. J.*, 2006, **91**, 3474-3481.
15. T. A. Doggett, G. Girdhar, A. Lawshe, D. W. Schmidtke, S. L.
40   Diamond and T. G. Diacovo, *Biophys. J.*, 2002, **83**, 194-205.
16. D. C. Duffy, J. C. McDonald, O. J. A. Schueller and G. M. Whitesides, *Anal. Chem.*, 1998, **70**, 4974-4984.
17. M. Bahrami, M. M. Yovanovich and J. R. Culham, *J. Fluids Eng.*, 2006, **128**, 1036-1044.
45 18. W. M. Deen, *AIChE J.*, 1987, **33**, 1409-1425.
19. H. L. Goldsmith and V. T. Turitto, *Thrombosis and haemostasis*, 1986, **55**, 415-435.
20. R. B. Bird, W. E. Stewart and E. N. Lightfoot, *Transport Phenomenon*, John Wiley and Sons, 1960.
50 21. C. Güell and R. H. Davis, *J. of Membrane Sci.*, 1996, **119**, 269-284.
22. V. Chen, *J. Membrane Sci.*, 1998, **147**, 265-278.
23. A. Bonnefoy, Q. Liu, C. Legrand and M. M. Forjmovic, *Biophys. J.*, 2000, **78**, 2834-2843.
24. E. M. Tracey and R. H. Davis, *J Colloid Interf Sci*, 1994, **167**, 104-
55   116.
25. J. Mueller and R. H. Davis, *J. of Membrane Sci.*, 1996, **116**, 47-60.
26. C. P. Beltran-Miranda, A. Khan, A. R. Jaloma-Cruz and M. A. Laffan, *Haemophilia*, 2005, **11**, 326-334.
27. M. E. Carr, E. J. Martin and S. L. Carr, *Blood Coagul. Fibrinolysis*,
60   2002, **13**, 193-197.
28. A. J. Marcus and L. B. Safier, *Faseb J*, 1993, **7**, 516-522.
29. J. de Jong, R. G. H. Lammertink and M. Wessling, *Lab Chip*, 2006, **6**, 1125-1139.
30. R. F. Ismagilov, J. M. K. Ng, P. J. A. Kenis and G. M. Whitesides,
65   *Anal. Chem.*, 2001, **73**, 5207-5213.
31. V. V. Abhyankar, M. A. Lokuta, A. Huttenlocher and D. J. Beebe, *Lab Chip*, 2006, **6**, 389-393.
32. L. I. Genes, N. V. Tolan, M. K. Hulvey, R. S. Martin and D. M. Spence, *Lab Chip*, 2007, **7**, 1256-1259.
70 33. H. Bang, W. G. Lee, J. Park, H. Yun, J. Lee, S. Chung, K. Cho, C. Chung, D. Han and J. K. Chang, *J. Micromech. Microeng*, 2006, **16**, 708-714.
34. C. Ho and A. L. Zydney, *J. of Membrane Sci.*, 1999, **155**, 261-275.
35. J. A. Hubbell and L. V. McIntire, *Biophys. J.*, 1986, **50**, 937-945.
75 36. B. J. Folie and L. V. McIntire, *Biophys. J.*, 1989, **56**.
37. E. N. Sorensen, G. W. Burgreen, W. R. Wagner and J. F. Antaki, *Ann. Biomed. Eng.*, 1999, **27**, 436-448.

**Table 1** The Darcy's permeability was measured for track-etched
polycarbonate membranes with an average pore diameter of 0.6 µm and 1
µm for three surface treatments; no treatments, incubation in 1 mg/mL
5 bovine serum albumin (BSA), incubation in 0.1 mg/mL fibrinogen. The
permeability values were calculated by a least squares fit of water
velocity as a function of pressure drop across the membrane for three
transmembrane pressures (Figure S1). The goodness-of-fit was measured
by the R^2 statistic.

Treatment	Pore Diameter (µm)	Darcy's Permeability[a] (nm²)	R^2
No coating	1	3720	0.97
BSA	1	3530	0.90
Fibrinogen	1	3690	0.90
No coating	0.6	905	0.97
BSA	0.6	965	0.97
Fibrinogen	0.6	519	0.90

10 [a] See Figure S1 for velocity versus pressure data.
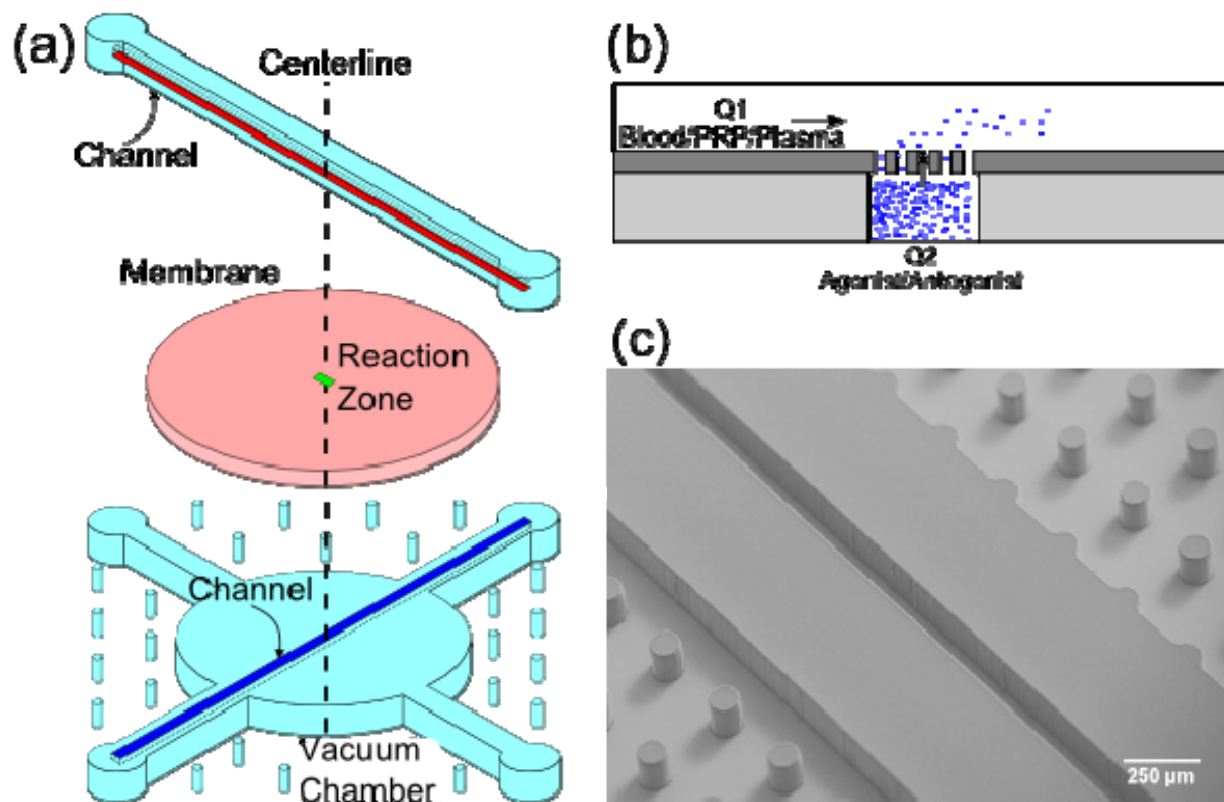
Fig. 1 (a) The device consisted of two perpendicular channels in PDMS separated by a polycarbonate membrane. The two PDMS layers are reversibly sealed using vacuum assisted bonding. (b) At the intersection of the two channels, the flux of the agonist molecules was controlled by the pore size and
5 transmembrane pressure. The transmembrane pressure was manipulated by varying the relative flow rate (Q1/Q2) between the top and bottom channels. (c) Electron micrograph of the bottom channel and posts in the vacuum chamber, which provided mechanical support during operation.
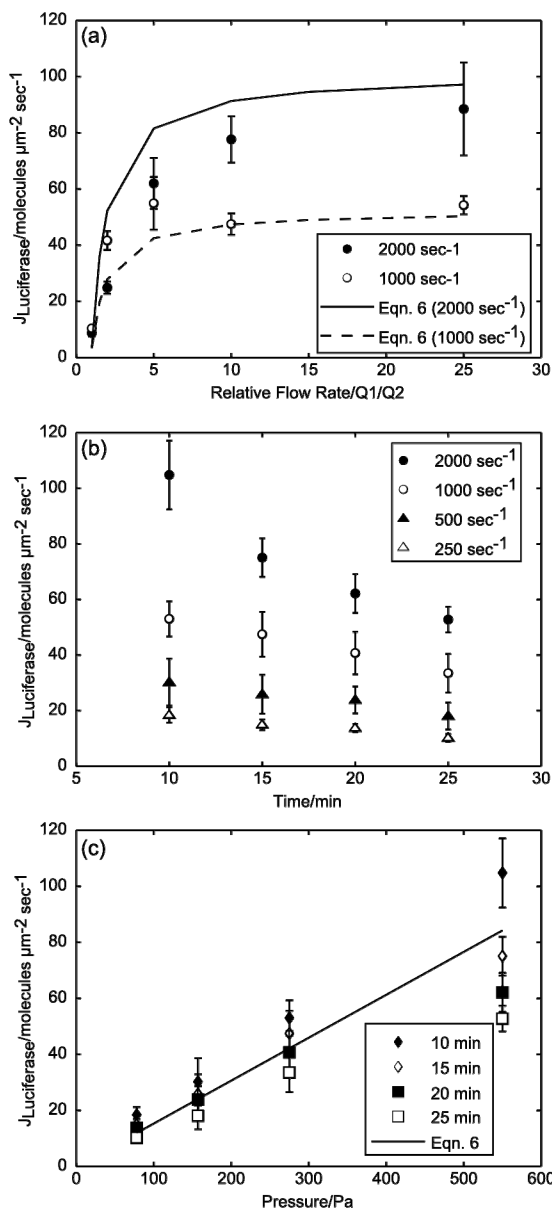
Fig. 2 (a) For the mean wall shear rates of 1000 sec^{-1} and 2000 sec^{-1} in the top channel, the flux was manipulated by changing the relative flow rate
[5] (Q1/Q2). The flow rate in the top channel, Q1, was held constant to achieve a desired wall shear rate, and Q2 was changed to vary the transmembrane pressure. The solid lines represent the luciferase flux predicted by eqn. 6. (b) The luciferase flux decreased with time due to fouling of the pores for wall shear rates of 250, 500, 1000, and 2000 sec^{-1}.
[10] (c) The flux data in (b) plotted as function of transmembrane pressure,. The line represents the predicted for a Darcy's permeability of 3690 nm[2]. Each data point represents the mean and the error bars represent the standard deviation (n=3).
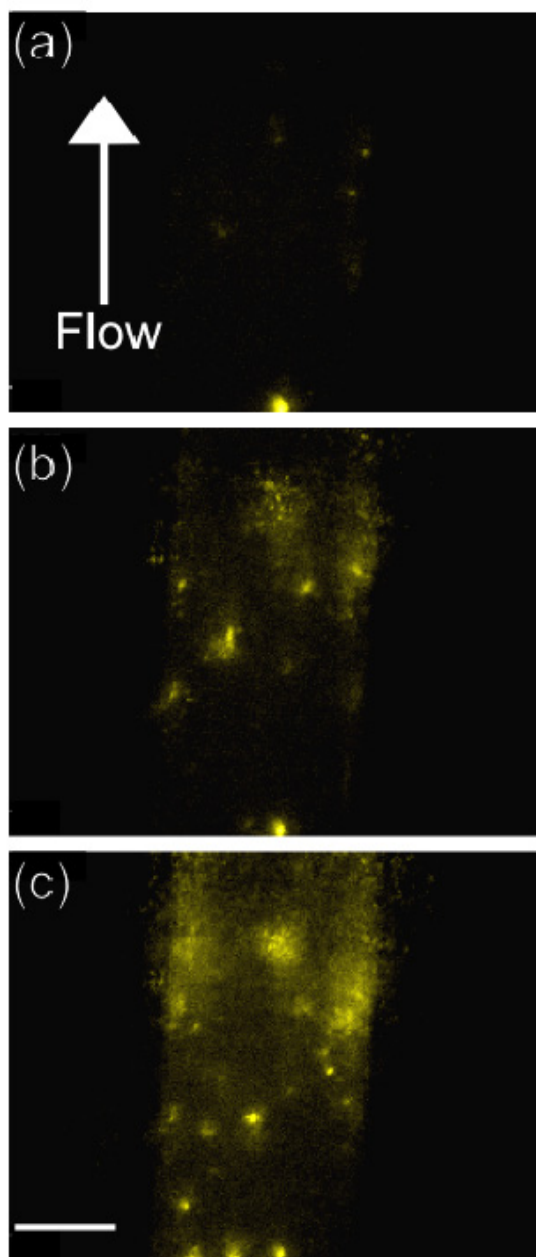
Fig. 3 Real-time fluorescence microscopy of platelet adhesion and aggregation for a mean wall shear rate of 250 sec^{-1}, 10 µM ADP in the bottom channel, and Q1/Q2=0.075 at (a) 1, (b) 3, and (c) 5 minutes. Scale bar=50 µm.
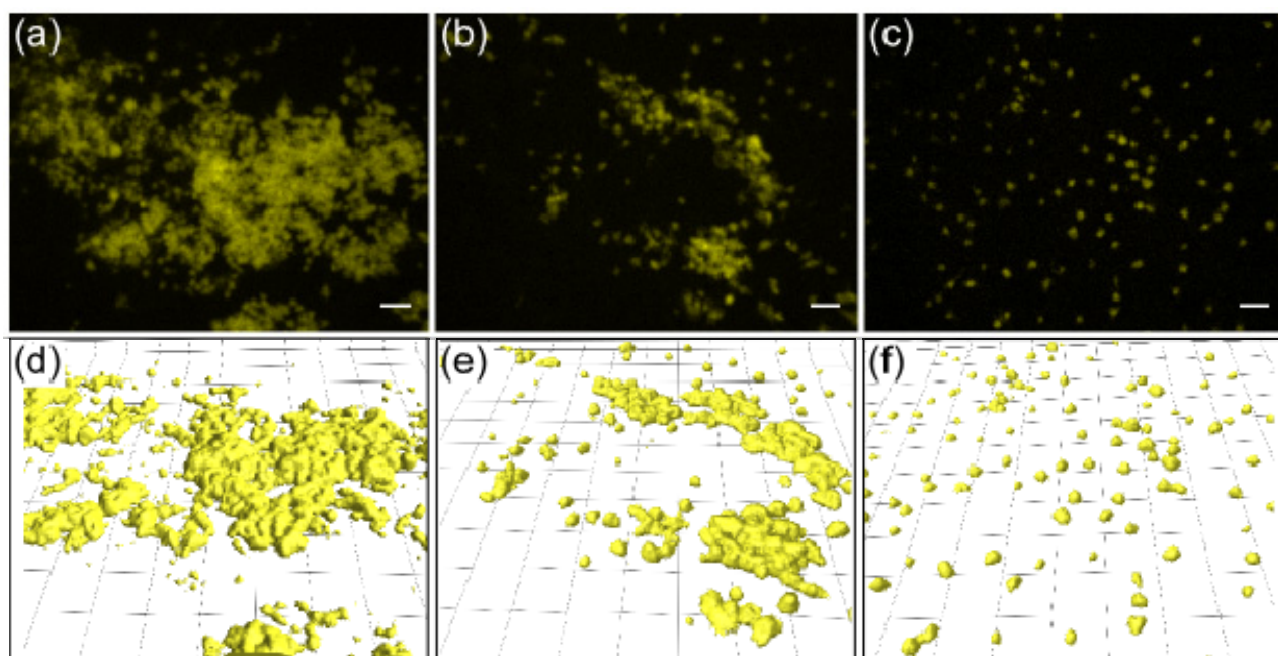
Fig. 4 Spinning disk confocal images (a-c) and volume reconstruction (d-f) of platelet aggregates formed by introducing ADP into flowing whole blood at a defined flux. (a,d) At the highest flux (4.4×10^{-18} mol μm^{-2} sec^{-1}), there were 2-3 layers of platelets and aggregates with 7a surface density of 0.31 ± 0.04 platelets μm^{-2}. (b,e) At the middle flux (2.4×10^{-18} mol μm^{-2} sec^{-1}) there were monolayers of platelets and aggregates with a surface density of 0.21 ± 0.05 platelets μm^{-2}. (c,f) At the lowest flux (1.5×1010^{-18} mol μm^{-2} sec^{-1}), no aggregates were observed, but there was platelet adhesion within the reaction zone. Scale bar=10 μm (a-c) and grid spacing=5 μm (d-f).
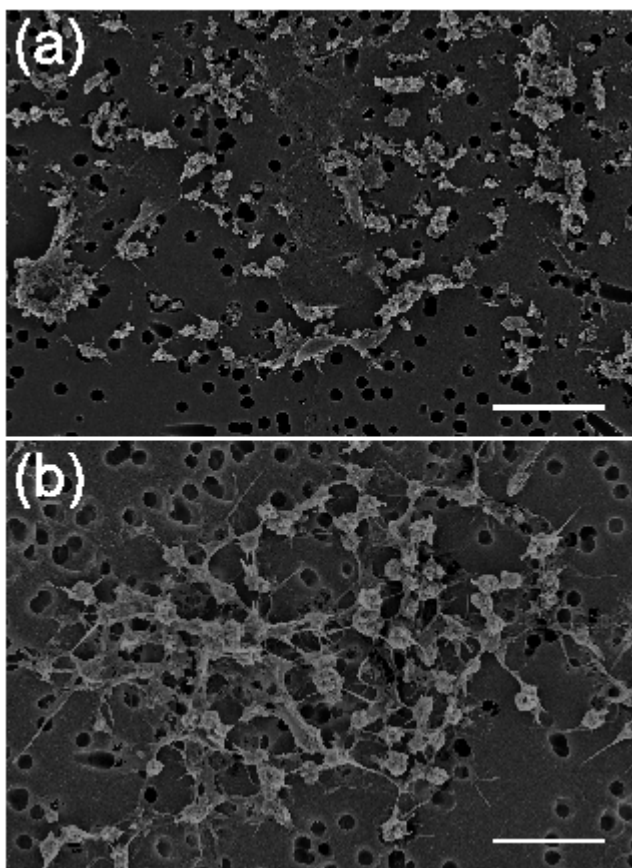
Fig. 5 Electron microscopy of adhered and aggregated platelets at the reaction zone. (a) At the lowest ADP flux (Q1/Q2=0.3), platelets adhered in singlets or small aggregates (2-5 cells). (b) At the higher ADP flux (Q1/Q2=0.15), platelets had multiple filopodia protruding from their cell bodies and formed aggregates. Scale bar=5 µm.
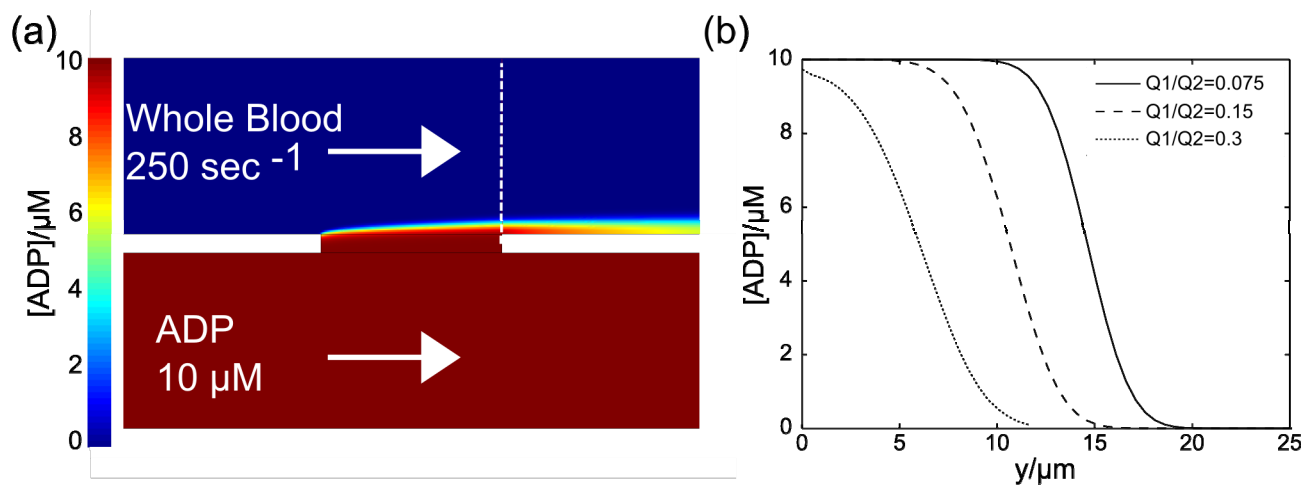
Fig. 6 : (a) Simulation of the boundary layer formed when ADP (Q1/Q2=0.15) was introduced into whole blood flowing at a wall shear rate of 250 sec⁻¹. (b) The simulation predicts that the thickness of the boundary layer increases with increasing ADP flux. The ADP concentration was plotted as a function of vertical distance, represented by the white line in (a), and relative flow rate at the edge of the reaction zone.
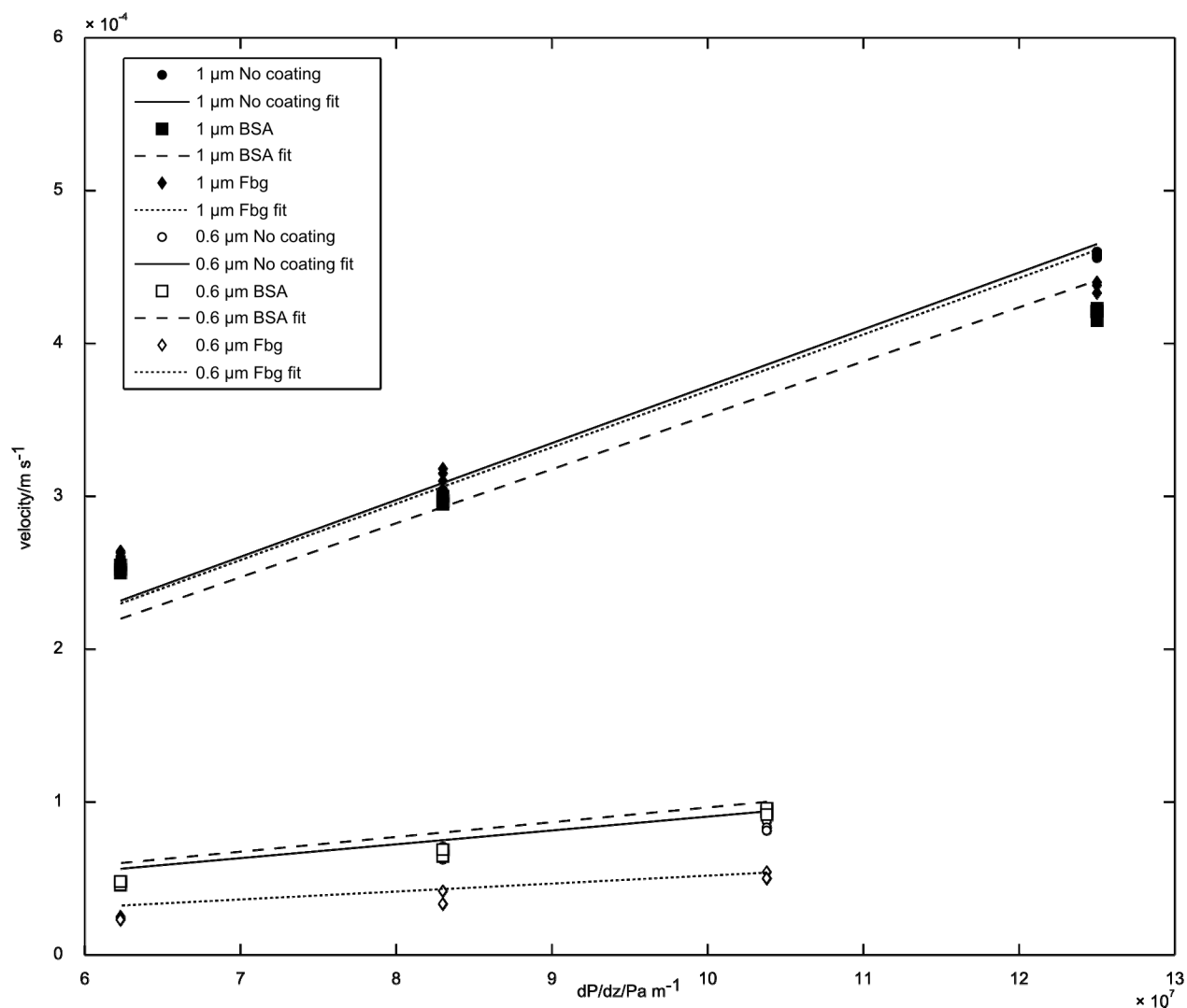
Fig S1 The hydraulic permeability of track-etched polycarbonate membranes was determined by a least squares fit of the velocity versus pressure drop (eqn. 5). Surface treatments of BSA and fibrinogen did not affect the permeability of membranes with a pore diameter of 1 μm. Fibrinogen treatment, but not BSA treatment, resulted in a decrease in permeability of membranes with a pore diameter of 0.6 μm.
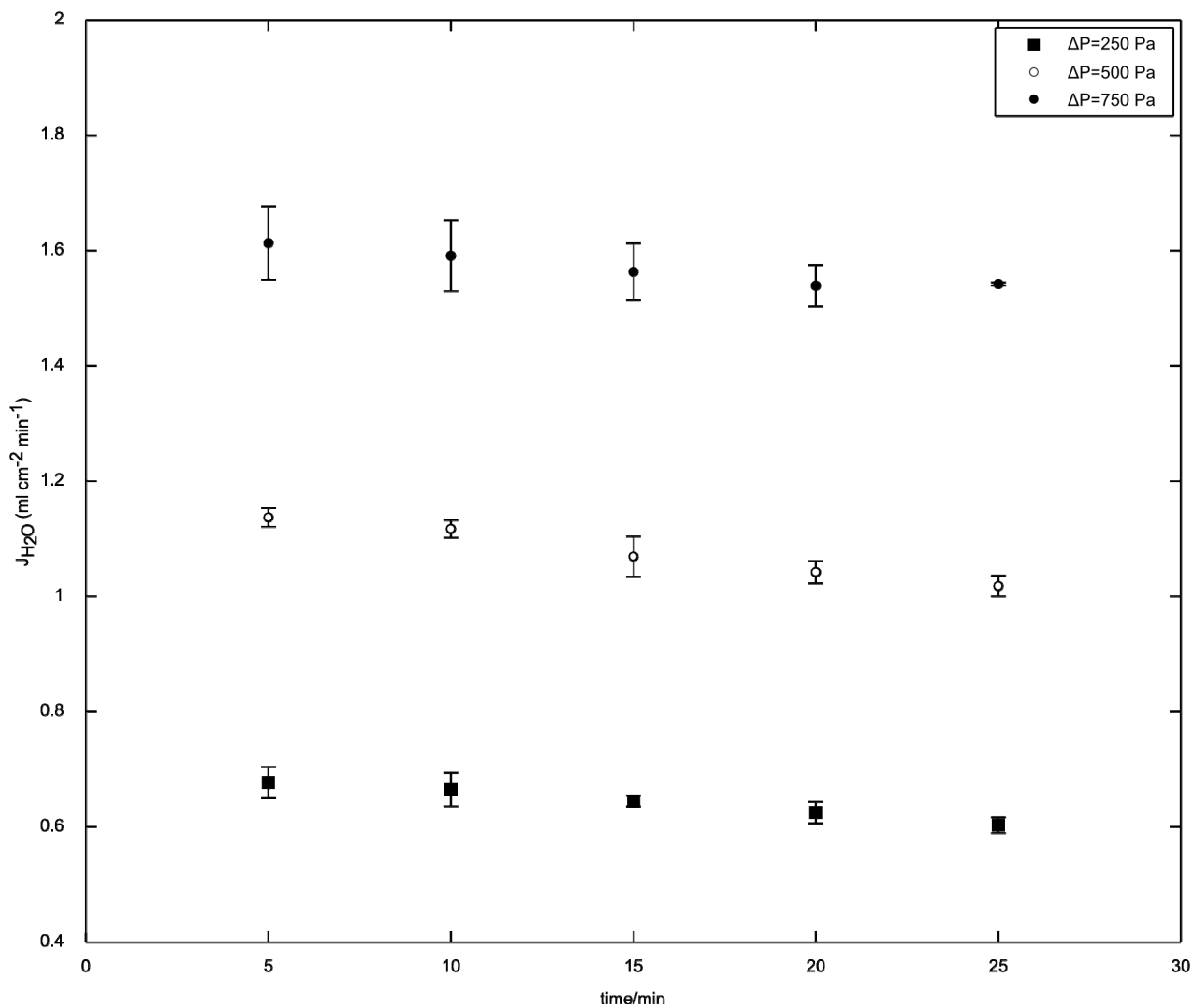
Fig. S2 The water flux through a track-etched polycarbonate membrane with a pore diameter of 1 mm. For constant pressure heads of 250, 500, and 750 Pa there was a 11.0%, 10.5%, and 4.4% decline in water flux over 25 minutes.

5

Contents Page
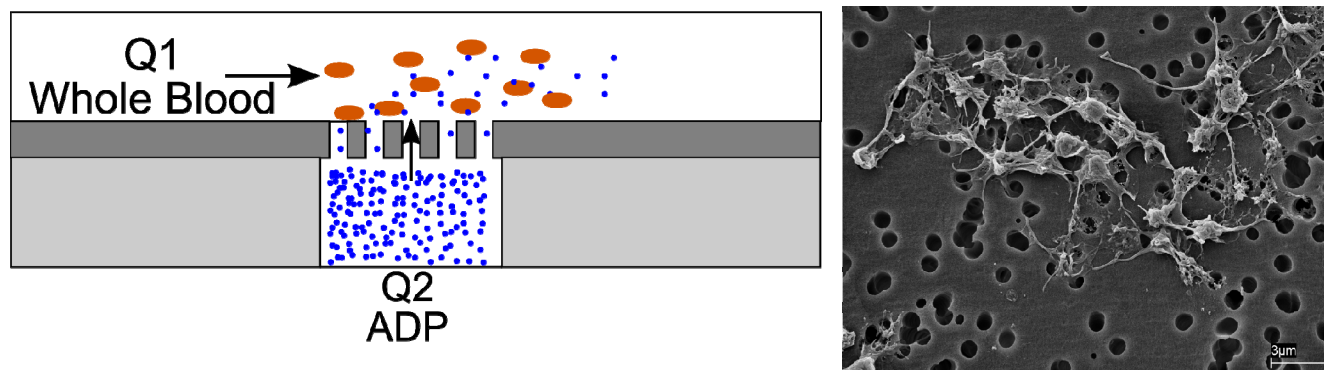
This report describes a membrane-based method for controlling the flux of soluble agonists into flowing blood. The device allows for real-time measurements of cellular adhesion and aggregation, as well as post hoc microscopy for examining aggregate morphology.